Strain Localization and Slip Instability in a Strain-Rate Hardening, Chemically Weakening Material

N. Brantut[1]
Department of Earth Sciences,
University College
London,
Rock and Ice Physics Laboratory,
WC1E 6BT London, UK;
Laboratoire de Géologie,
CNRS UMR 8538
École Normale Supérieure,
24 rue Lhomond,
75005 Paris, France
e-mail: nicolas.brantut@normalesup.org

J. Sulem
CERMES, UR Navier
École des Ponts ParisTech,
Université Paris-Est,
6, 8 avenue Blaise Pascal,
77455 Marne-la-Vallée Cedex 2, France
e-mail: jean.sulem@enpc.fr

The stability of steady slip and homogeneous shear is studied for rate-hardening materials undergoing chemical reactions that produce weaker materials (reaction-weakening process), in drained conditions. In a spring-slider configuration, a linear perturbation analysis provides analytical expressions of the critical stiffness below which unstable slip occurs. In the framework of a frictional constitutive law, numerical tests are performed to study the effects of a nonlinear reaction kinetics on the evolution of the instability. Slip instabilities can be stopped at relatively small slip rates (only a few orders of magnitude higher than the forcing velocity) when the reactant is fully depleted. The stability analysis of homogeneous shear provides an independent estimate of the thickness of the shear localization zone due to the reaction weakening, which can be as low as 0.1 m in the case of lizardite dehydration. The potential effect of thermo-chemical pore fluid pressurization during dehydration is discussed, and shown to be negligible compared to the reaction-weakening effect. We finally argue that the slip instabilities originating from the reaction-weakening process could be a plausible candidate for intermediate depth earthquakes in subduction zones. [DOI: 10.1115/1.4005880]

1 Introduction

Rock forming minerals undergo chemical reactions and phase changes as pressure and temperature conditions vary during burial and exhumation cycles. These mineral changes can affect the mechanical behavior of rocks, and thus modify the way they accommodate tectonic stress and strain. Generally, the mineral assemblage that forms during the reaction has different mechanical properties from the starting assemblage, and can be either stronger (reaction hardening) or weaker (reaction weakening). Reaction weakening behavior has been extensively documented in the case of rocks containing dehydrating minerals, such as serpentinite or gypsum. Such thermal decomposition reactions constitute an important class of mineral transformations that is thought to play an important role in the earth's tectonics [1,2].

These chemical reactions can affect the mechanical properties of rocks in a number of ways: (1) they release volatiles (fluid phase), (2) they result in a negative solid volume change (porosity increase), and (3) the newly formed minerals generally have different mechanical properties from the starting materials. Effect (1) has been largely documented experimentally (e.g., Refs. [1–5]) and theoretically (e.g., Refs. [6, 7]), and is related to the change in effective stress applied on the fault that produces an apparent weakening; it can be considered as an extrinsic weakening process, as it does not affect the strength of the material itself. Effect (3), which is an actual intrinsic reaction weakening behavior, has mostly been reported from a series of experimental studies on porous (and thus permeable) serpentinite aggregates [8–11]. In these tests, evidences of ultra-fine grained superplastic olivine have been reported during deformation of a serpentinite aggregate at the dehydration temperature of serpentinite. This intrinsic weakening mechanism is observed only at low strain rates, below

10^{-5} s^{-1}: deformation experiments performed at larger strain rates do not exhibit any weakening related to the reaction [10,12,13].

The problem addressed in the present paper is the possibility of localization and slip instability in a reactive material undergoing shear at the onset of a chemical reaction. We first derive the general governing and constitutive equations, in the drained regime. Second, we test the stability of slip across a shear zone that is loaded remotely through an elastic body (in the well-known spring-slider configuration). Using the same governing laws, we then test the stability of homogeneous shear to spatial perturbations in order to detect the possibility of shear localization and estimate the thickness of the localized shear zone. The potential effect of pore fluids is then investigated. Finally, the geophysical implications of the reaction-weakening behavior are discussed.

2 Model Description

We consider a fully saturated layer of rock containing reactive minerals undergoing shear deformation under drained conditions. The deforming layer thickness is denoted h and is assumed to be much smaller than the surrounding crustal block. The shear loading is performed through an elastic medium, in the spring-slider configuration (Fig. 1). We analyze here a 1D problem and consider the variations of the various thermo-poro-mechanical quantities only in the direction normal to the layer (coordinate y).

2.1 Momentum Balance. At slow strain rates, inertial effects can be neglected. Hence, the shear stress τ and the normal stress σ are uniform throughout the layer. In particular we have:

$$\frac{\partial \tau}{\partial y} = 0 \qquad (1)$$

The material inside the shear band undergoes inelastic loading whereas the external loading block remains elastic. Continuity of shear stress at the boundary of the shear zone implies that $\tau = k(\delta_\infty - \delta)$, where k is the spring stiffness (measured in Pa/m),
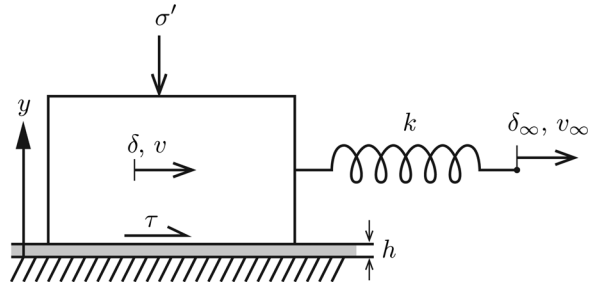
Fig. 1 Schematic of the spring-slider configuration. The fault zone (thickness *h*) is loaded remotely through an elastic medium of equivalent stiffness *k*. The constant effective normal stress is $\sigma' = \sigma - p$, where *p* is the pore pressure.

δ_∞ is the displacement applied remotely (at the loading end of the spring), and δ is the net slip displacement at the boundary of the shear zone. In terms of stress and slip rate we thus obtain

$$\frac{\partial \tau}{\partial t} = k(v_\infty - v) \tag{2}$$

where ν_∞ is the remotely applied slip rate and ν is the slip rate on the shear zone.

2.2 Energy Balance. The temperature evolution $T(y,t)$ is given by the equation of energy conservation inside the shear layer. Heat is generated by dissipation of mechanical energy (shear heating), and is partitioned into temperature increase and reaction enthalpy, which is a heat sink when the reaction is endothermic. We assume here that all the mechanical work is converted into heat, i.e., the Taylor-Quinney coefficient is assumed to be 1. Denoting m_0 the mass of reacting mineral per unit of total rock volume, ΔH the reaction enthalpy per unit mass of reactant and μ the extent of completion of the reaction, we obtain [7,14,15]

$$\frac{\partial T}{\partial t} = \frac{\tau \dot{\gamma}}{\rho C} + d_{\text{th}} \frac{\partial^2 T}{\partial y^2} - m_0 \frac{\Delta H}{\rho C} \frac{\partial \mu}{\partial t} \tag{3}$$

where τ is the applied shear stress on the fault, $\dot{\gamma}$ is the strain rate, ρ is the bulk density of the rock, C is the heat capacity of the rock, and d_{th} is the heat diffusivity. We emphasize here that the convention of $\Delta H > 0$ is taken for endothermic reactions; hence the negative sign of the chemical source term on the right-hand-side of Eq. (3).

For a constant shear zone thickness h and a given slip rate ν at the boundary of the shear zone, the strain rate is written $\dot{\gamma} = v/h$.

2.3 Reaction Rate. The reaction rate is assumed to be of first order, with a temperature dependency following an Arrhenius law:

$$\frac{\partial \mu}{\partial t} = A(1 - \mu) \exp\left(-\frac{E_a}{RT}\right) \tag{4}$$

where A is a pre-exponential constant, E_a is the activation energy of the reaction, and R is the gas constant. Although probably too simplistic, the formulation of Eq. (4) allows us to explore two fundamental characteristics of the chemical reaction: temperature dependency and depletion.

One drawback of the Arrhenius formulation is that the reaction rate is never exactly zero. Thus, over the long term, the reaction will occur even at very low temperature, whereas it should be thermodynamically prohibited. One way to overcome this inconsistency is
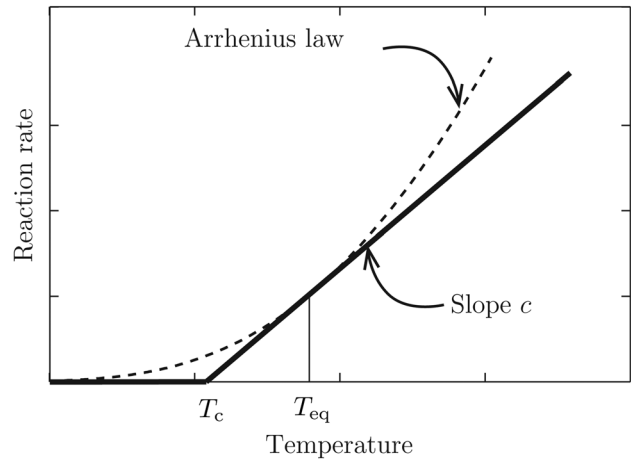

Fig. 2 Linearization of the Arrhenius law around T_{eq}; the cutoff temperature T_c is the intersect of the slope with the *T* axis

to introduce a cutoff temperature T_c below which the reaction rate is assumed to be identically zero. To avoid any discontinuous jump in the reaction rate at T_c, the reaction rate is linearized in temperature immediately above T_c. The linearization procedure is depicted graphically in Fig. 2. In addition, we also linearize the kinetics in reaction extent.

Formally we have

$$\frac{\partial \mu}{\partial t} \approx \begin{cases} 0 & \text{if} \quad T < T_c \\ c_T(T - T_c) - c_\mu \mu & \text{if} \quad T_c \leq T \end{cases} \tag{5}$$

where c_T and c_μ are the first order coefficients of the Taylor expansion of the kinetics law around $T = T_{\text{eq}} > T_c$ and $\mu = \mu_0$:

$$c_T = A(1 - \mu_0) \frac{E_a}{RT_{\text{eq}}^2} \exp\left(-E_a/(RT_{\text{eq}})\right) \tag{6}$$

$$c_\mu = A \exp\left(-E_a/(RT_{\text{eq}})\right) \tag{7}$$

From the definition of T_c given above, we have

$$T_c = T_{\text{eq}}(1 - T_{\text{eq}}/(E_a/R)) \tag{8}$$

2.4 Constitutive Model. We assume that the shear stress τ is a function of applied effective normal stress σ', strain rate $\dot{\gamma}$ and reaction extent μ:

$$\tau = \tau(\sigma', \dot{\gamma}, \mu) \tag{9}$$

Small perturbation of shear stress are thus of the form

$$\delta \tau = \frac{\partial \tau}{\partial \sigma'} \delta \sigma' + \frac{\partial \tau}{\partial \dot{\gamma}} \delta \dot{\gamma} + \frac{\partial \tau}{\partial \mu} \delta \mu \tag{10}$$

Here we focus on the rate-hardening, reaction-weakening case, which means that we assume

$$\frac{\partial \tau}{\partial \dot{\gamma}} > 0 \text{ (rate hardening)}, \quad \frac{\partial \tau}{\partial \mu} < 0 \text{ (reaction weakening)} \tag{11}$$

These features are schematically shown in Fig. 3. In a linear stability analysis, these general assumptions are sufficient to detect the onset of localization and unstable slip. However, in numerical simulations we need to assume an explicit form of the constitutive law. This choice is given as follows.
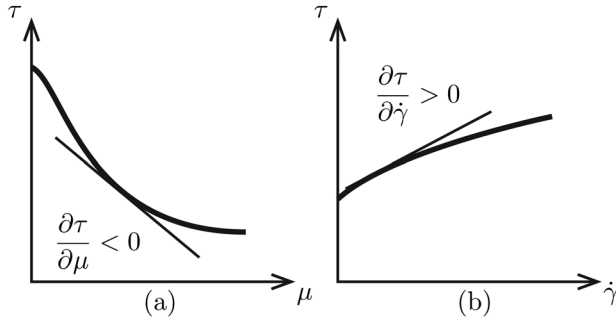
Fig. 3 Constitutive relation for the reacting rock. (*a*) For constant strain rate, the shear stress decreases as reaction progresses. (*b*) At a given extent of reaction, the shear stress increases with increasing strain rate.

We assume fully drained condition (i.e., no pore pressure change), and constant normal stress. The constitutive law is written in terms of friction coefficient *f*,

$$\tau = f(\dot{\gamma}, \mu)\sigma' \tag{12}$$

where

$$\frac{\partial f}{\partial \dot{\gamma}} > 0 \ \text{(rate hardening)}, \quad \frac{\partial f}{\partial \mu} < 0 \ \text{(reaction weakening)}$$

This description has its roots in the general rate-and-state formulation of friction, where the "state" has been identified to the reaction extent. An explicit, although less general, constitutive formulation can then be assumed in the form

$$f(\dot{\gamma}, \mu) = f_0 + a \ln(\dot{\gamma}/\dot{\gamma}_0) - b\mu \tag{13}$$

where f_0 is a reference friction coefficient, $a > 0$ and $b > 0$ are constitutive parameters of the friction law, and $\dot{\gamma}_0$ is a reference strain rate.

The parameter *a* corresponds to the so-called "direct effect," which is based on the activation energy for sliding at asperities [16–18]. The parameter *b* can be simply understood as the potential change in friction coefficient from the initial mineral assembly (e.g., pure serpentine) to the new mineral assembly after the reaction (fine-grained olivine and talc). In this framework, the "evolution law" of the state variable is simply given by the reaction kinetics (coupled to the heat equation).

This formulation is certainly oversimplified as compared to the true frictional response, in the sense that the reaction weakening is only observed experimentally at low strain rates (below 10^{-5} s^{-1}, see Refs. [8, 10]): the value of *b* should be velocity dependent in such a way that, at high strain rates, the friction coefficient comes back to its value prior to dehydration. Moreover, it does not take into account the large strain hardening commonly observed during serpentinite dehydration (probably due to compaction of the new mineral assembly, and olivine grain growth). However, Eq. (13) provides the appropriate phenomenological friction law at least to study the initiation of such dehydration reactions.

3 Nucleation of Slip Instability

3.1 Summary of Governing Equations and Normalization. Taking into account all the simplifications and assumptions described in Sec. 2, the system of equations governing temperature, reaction extent, and stress on the fault becomes

$$\frac{\partial T}{\partial t} = d_{\text{th}}\frac{\partial^2 T}{\partial y^2} + \frac{\tau v}{\rho C h} - m_0 \frac{\Delta H}{\rho C}\frac{\partial \mu}{\partial t} \tag{14}$$

$$\frac{\partial \mu}{\partial t} = c_T(T - T_{\text{c}}) - c_\mu \mu \tag{15}$$

$$\frac{\partial \tau}{\partial t} = k(v_\infty - v) \tag{16}$$

Let us introduce the following notations:

$$v = v_\infty \tilde{v} \tag{17}$$

$$t = \frac{h}{v_\infty}\tilde{t} \tag{18}$$

$$y = h\tilde{y} \tag{19}$$

$$T = T_a \tilde{T} \tag{20}$$

$$\tau = \tau_0 \tilde{\tau} \tag{21}$$

where $T_a = E_a/R$ and τ_0 is a reference shear stress. In the frictional framework described in Eqs. (12) and (13), the reference shear stress is $\tau = f_0\sigma'$. The governing equations are rewritten as:

$$\frac{\partial \tilde{T}}{\partial \tilde{t}} = \mathbb{D}_{\text{th}}\frac{\partial^2 \tilde{T}}{\partial \tilde{y}^2} + \mathbb{H}\tilde{\tau}\tilde{v} - \mathbb{T}\frac{\partial \mu}{\partial \tilde{t}} \tag{22}$$

$$\frac{\partial \mu}{\partial \tilde{t}} = \mathbb{C}_T(\tilde{T} - \tilde{T}_{\text{c}}) - \mathbb{C}_\mu \mu \tag{23}$$

$$\frac{\partial \tilde{\tau}}{\partial \tilde{t}} = \mathbb{K}(1 - \tilde{v}) \tag{24}$$

where the following non-dimensional numbers were used:

$$\mathbb{D}_{\text{th}} = d_{\text{th}}/(hv_\infty) \tag{25}$$

$$\mathbb{H} = \tau_0/(\rho C T_a) \tag{26}$$

$$\mathbb{T} = m_0 \Delta H/(\rho C T_a) \tag{27}$$

$$\mathbb{C}_T = c_T T_a h/v_\infty \tag{28}$$

$$\mathbb{C}_\mu = c_\mu h/v_\infty \tag{29}$$

$$\mathbb{K} = kh/\tau_0 \tag{30}$$

3.2 Stability Condition. The stationary solution of the system corresponds to $\tilde{v}_0 = 1$. The interesting situation, relevant to fault slip at depth in the Earth, is when the fault is sliding stably *before* the chemical reaction significantly starts. This is obviously the case here since we assumed pure velocity strengthening behavior of the material. The question addressed here is whether a small perturbation at the onset of the chemical reaction can drive a slip rate instability. The solution we look at needs to be constrained by $\tilde{T}_0 = \tilde{T}_{\text{c}}$ and $\mu_0 = 0$, and hence $\tilde{\tau}_0 = 1$. The stationary temperature profile is a parabola: $\tilde{T} = -\mathbb{H}/(2\mathbb{D}_{\text{th}})\tilde{y}^2 + \tilde{T}_{\text{c}}$.

This is physically valid only for a unique remote boundary condition in temperature (otherwise the temperature becomes negative far from the fault). In the following, we only investigate adiabatic perturbations, which can be seen as the most critical situation (heat diffusion will have a stabilizing effect), and the initial temperature profile does not play any role.

Let us investigate the behavior of infinitesimal, adiabatic perturbations $(\tilde{T}_1, \mu_1, \tilde{v}_1)$ around the stationary solution. The perturbations satisfy the linearized system

$$\frac{\partial \tilde{T}_1}{\partial \tilde{t}} = \mathbb{H}((1 + \alpha)\tilde{v}_1 - \beta\mu_1) - \mathbb{T}\frac{\partial \mu_1}{\partial \tilde{t}} \tag{31}$$

$$\frac{\partial \mu_1}{\partial \tilde{t}} = \mathbb{C}_T\tilde{T}_1 - \mathbb{C}_\mu\mu_1 \tag{32}$$

$$\alpha\frac{\partial \tilde{v}_1}{\partial \tilde{t}} - \beta\frac{\partial \mu_1}{\partial \tilde{t}} = -\mathbb{K}\tilde{v}_1 \tag{33}$$

where we recall that

$$\alpha = \frac{\partial \tilde{\tau}}{\partial \tilde{v}}\bigg|_{\tilde{v}_0, \mu_0} \tag{34}$$

$$\beta = -\frac{\partial \tilde{\tau}}{\partial \mu}\bigg|_{\tilde{v}_0, \mu_0} \tag{35}$$

Equations (31), (32), and (33) form a linear system of partial differential equations. We look for solutions of the form

$$\begin{pmatrix} \tilde{T}_1 \\ \mu_1 \\ \tilde{v}_1 \end{pmatrix} = \begin{pmatrix} B_1 \\ B_2 \\ B_3 \end{pmatrix} \exp(s\tilde{t}) \tag{36}$$

where s is the growth rate of the perturbation and the B_i are constants. The linear system has a non-trivial solution $(B_1, B_2, B_3) \neq (0,0,0)$ if its determinant is identically zero; this condition gives a characteristic polynomial equation for the growth rate s:

$$s^3 + s^2(\mathbb{C}_T\mathbb{T} + \mathbb{C}_\mu + \mathbb{K}/\alpha) + s((\mathbb{C}_T\mathbb{T} + \mathbb{C}_\mu)\mathbb{K}/\alpha - \mathbb{C}_T\mathbb{H}\beta/\alpha) + \mathbb{C}_T\mathbb{H}\beta\mathbb{K}/\alpha = 0 \tag{37}$$

Equation (37) is cubic in s and explicit formulas exist to obtain its roots. However, we do not need the explicit expression of the roots but only their signs. This can be done for instance by Descartes' rule of signs. It can thus be proven that Eq. (37) has only negative roots if

$$\mathbb{K} \geq \mathbb{K}_{cr} = \frac{\mathbb{C}_T\mathbb{H}\beta}{\mathbb{C}_\mu + \mathbb{C}_T\mathbb{T}} \tag{38}$$

The inequality represented in Eq. (38) is the stability condition of the linearized system. A more endothermic reaction tends to stabilize the system (lower $\mathbb{K}_{cr}$.). On the other hand, larger heat generation (parameter $\mathbb{H}$) and larger reaction weakening tend to destabilize further the system. The stability condition in Eq. (38) does not involve the rate-hardening parameter α. Although intuitively unexpected, this can be understood from the fact that larger rate-hardening induces larger shear heating and thus faster reaction rate, which ends up in larger reaction-weakening. Further calculations indicate that α appears as a stabilizing factor in the stability condition if heat diffusion is included (for instance using a membrane approximation). In any event, although α may not necessarily enter in the stability condition, it has an influence on the actual value of the growth rate, and we expect fast growth rates (i.e., small s) when α is large.

The inequality in Eq. (38) is used to define a critical value, $\mathbb{K}_{cr}$ or equivalently a critical stiffness k_{cr}, below which the fault motion is unstable. Using dimensional parameters, this critical stiffness is

$$k_{cr} = \frac{\tau_0}{h} \frac{\tau_0\beta}{\rho C T_{eq}^2/T_a + m_0\Delta H} \tag{39}$$

3.3 Numerical Example.

A representative case discussed in the introduction is that of lizardite dehydration reaction into talc, forsterite and water:

$$5Mg_3Si_2O_5(OH)4 \rightarrow Mg_3Si_4O_{10}(OH)_2 + 6Mg_2SiO_4 + 9H_2O \tag{40}$$
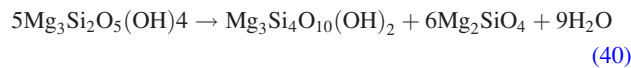
The reaction enthalpy is calculated from standard enthalpies of formation (values obtained in Refs. [19, 20]) and is $\Delta H = 0.24$ MJ/kg. For a rock containing 10 wt% lizardite, the mass of lizardite per unit of rock mass is $m_0 \approx 250$ kg/m^3. The kinetic parameters are extracted from laboratory data obtained on solid [21], and are $A = 2.91\ 10^{32}$/s and $E_a = 528$ kJ/mol. The equilibrium temperature

is assumed to be $T_{eq} = 450$ °C. At the onset of the reaction, $\mu_0 = 0$, and we obtain $c_T = 2.5\ 10^{-5}$/°C/s and $c_\mu = 2.1\ 10^{-6}$/s. The specific heat capacity of the fault rock is around 2.7 MPa/°C. In the framework of a frictional constitutive law, the rate strengthening effect α can be estimated from velocity stepping tests performed in the laboratory. The so-called direct effect a is of the order of 0.01, thus a normalized rate strengthening parameter of $\alpha = a/f_0 \approx 0.02$ is representative of serpentine rich fault rock [22]. The reaction weakening parameter β is not constrained by any direct experimental data. However, Ref. [10] mentions that the yield strength of dehydrating serpentinite at strain rate less than 10^{-6}/s is effectively zero. Thus a representative, conservative estimate of β can be of the order of 0.8, i.e., the fully reacted material is 80% weaker than the intact one. The reference shear stress τ_0 depends on the initial effective normal stress σ' and the initial friction coefficient f_0 (see Eq. (12)). At a depth of around 30 km, a representative value of $\tau_0 \approx 200$ MPa is chosen. Finally, we set a shear zone thickness of $h = 1$ m and a remotely applied velocity of the order of a tectonic plate velocity, i.e., $v_\infty = 10^{-9}$ m/s. This set of values (reported in Table 1) is used to calculate the non-dimensional parameters appearing in Eq. (38).

In order to test the validity of the linear stability analysis, the system can be solved numerically with the nonlinear reaction kinetics. The cutoff temperature and a subsequent linear temperature dependence up to T_{eq} is still needed to avoid reaction progress at unrealistically low temperature, but the full Arrhenius law is used above T_{eq} and the depletion is always taken into account:

$$\frac{\partial \mu}{\partial t} = \begin{cases} 0 & \text{if } T < T_c \\ A\frac{T_{eq}^2}{T_a}\exp(-T_a/T_{eq})(1-\mu)(T-T_c) & \text{if } T_c \leq T < T_{eq} \\ A(1-\mu)\exp(-T_a/T) & \text{if } T_{eq} \leq T \end{cases} \tag{41}$$

This kinetic law is schematically shown in Fig. 4. The system of Eqs. (22), (23), and (24) is solved using MATLAB's ODE15S routine. The parameter values are given in Table 1. The stability condition is then

$$\mathbb{K}_{cr} = 2.43, \quad \text{i.e.,} \quad k_{cr} = 5.84 \times 10^8 \text{Pa/m}$$

We test four different values of spring stiffnesses across the transition to stability, $k = 3 \times 10^6$ Pa/m, $k = 3 \times 10^8$ Pa/m, $k = 6 \times 10^8$ Pa/m and $k = 3 \times 10^9$ Pa/m. The results are reported in Fig. 5. It confirms that for $k > k_{cr}$ the motion is stable, whereas it is not for $k > k_{cr}$. Interestingly, the instability arising close to

Table 1 Parameter values used for the stability analysis of fault slip. Reaction enthalpy is calculated from standard enthalpies of formation for the lizardite dehydration reaction [19,20]. Kinetics data correspond to the dehydration reaction of solid cylinders of lizardite [21].

| Parameter	Symbol	Value	Unit
Friction coefficient	f_0	0.6	
Rate strengthening parameter	a	0.002	
Reaction weakening parameter	b	0.5	
Specific heat capacity	ρC	2.7×10^6	Pa °C^{-1}
Shear zone width	h	1	m
Initial effective stress	σ'	400×10^6	Pa
Initial temperature	T_0	440	°C
Mass of reacting mineral	m_0	250	kg m^{-3}
Remote slip rate	v_∞	10^{-9}	m s^{-1}
Enthalpy change	ΔH	0.24×10^6	J kg^{-1}
Thermal diffusivity	d_{th}	10^{-6}	m^2 s^{-1}
Pre-exponential factor	A	2.91×10^{32}	s^{-1}
Activation energy	E_a	528×10^3	kJ mol^{-1}
Equilibrium temperature	T_{eq}	450	°C
Cutoff temperature	T_c	442	°C
Thermal dependency of kinetics	c_T	2.54×10^{-5}	°C^{-1}s^{-1}
Depletion dependency of kinetics	c_μ	2.10×10^{-6}	s^{-1}
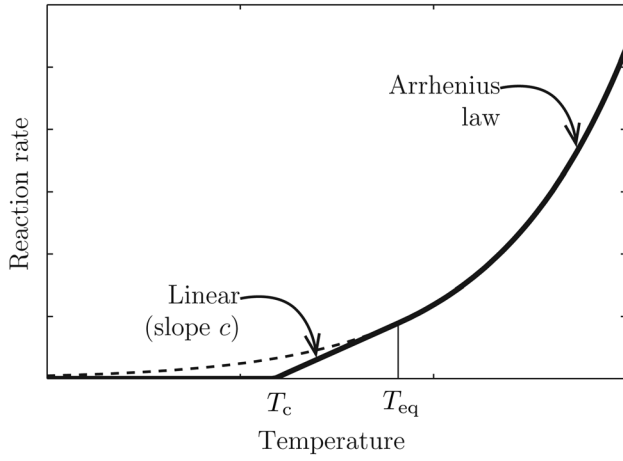
Fig. 4 Regularized reaction kinetics used in the numerical stability analysis
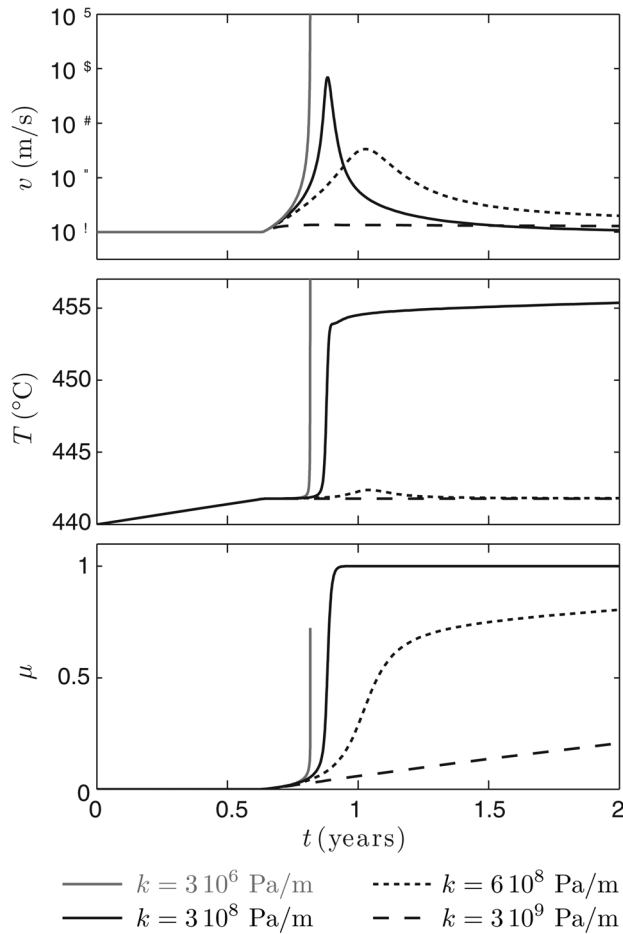

Fig. 5 Numerical illustration of the transition from slip instability (solid red and black lines) to slip stability (dotted and dashed block lines). The critical stiffness calculated from Eq. (39) is $k_{cr} = 5.75 \times 10^8$ Pa/m. For $k = 3 \times 10^8$ Pa/m (solid black line), the growth rate of the instability is low, and the reactant is rapidly fully depleted.

the transition are short-lived, because the reaction is rapidly depleted and the source of the instability then vanishes. A similar behavior is observed well inside the instability field ($k = 3 \times 10^6$ Pa/m) for high values of α: in that case, the stability condition is unchanged but the growth rate of the instability becomes much

slower, allowing complete depletion of the reactant before the slip rate reaches dramatically high values.

The value of k_{cr}, and thus the stability, always depends on the ratio τ_0/h. Thinner sheared layers require a higher stiffness of the spring for stable slip. As explained previously, the shear stress level τ_0 can be estimated from the friction coefficient and the effective normal stress at the considered depth. However, the shear zone thickness h is not constrained by any direct measurement or calculation, and we simply assumed a constant value throughout the calculations. In the following section, we investigate the possibility of strain localization within the reactive material during loading, in order to estimate the thickness of the shear zone which could result from a strain localization process.

4 Strain Localization and Thickness of Shear Zone

4.1 Governing Equations Inside the Shear Zone. Stepping back from the spring-slider configuration investigated in the previous section, we study here the strain rate evolution in space inside a layer of reacting rock sheared at a given nominal strain rate $\dot{\gamma}_0$. Without simplification on the heat diffusion, the governing equations are

$$\frac{\partial T}{\partial t} = \frac{\tau \dot{\gamma}}{\rho C} + d_{th} \frac{\partial^2 T}{\partial y^2} - m_0 \frac{\Delta H}{\rho C} \frac{\partial \mu}{\partial t} \tag{42}$$

$$\frac{\partial \mu}{\partial t} = c_T(T - T_c) - c_\mu \mu \tag{43}$$

$$\frac{\partial \tau}{\partial y} = 0 \tag{44}$$

The system can be normalized by using $1/\dot{\gamma}_0$ as a time scale and $\sqrt{d_{th}/\dot{\gamma}_0}$ as a space scale. The non-dimensional variables are then

$$\dot{\gamma} = \tilde{\dot{\gamma}}\dot{\gamma}_0 \tag{45}$$

$$t = \tilde{t}/\dot{\gamma}_0 \tag{46}$$

$$y = \tilde{y}\sqrt{d_{th}/\dot{\gamma}_0} \tag{47}$$

$$T = \tilde{T}T_a \tag{48}$$

$$\tau = \tilde{\tau}\tau_0 \tag{49}$$

The set of governing equations is then rewritten as

$$\frac{\partial \tilde{T}}{\partial \tilde{t}} = \frac{\partial^2 \tilde{T}}{\partial \tilde{y}^2} + \mathbb{H}\tilde{\tau}\tilde{\dot{\gamma}} - \mathbb{T}\frac{\partial \mu}{\partial \tilde{t}} \tag{50}$$

$$\frac{\partial \mu}{\partial \tilde{t}} = \mathbb{C}_T(\tilde{T} - \tilde{T}_c) - \mathbb{C}_\mu \mu \tag{51}$$

$$\frac{\partial \tilde{\tau}}{\partial \tilde{y}} = 0 \tag{52}$$

where we used the non-dimensional numbers defined in expressions in Eqs. (26), (27), (28) and (29).

4.2 Localization Wavelength Selection. Let us call $\tilde{T}_0$, μ_0 the *spatially uniform* (adiabatic) normalized temperature and reaction extent satisfying Eqs. (50), (51), and (52) at a given time during deformation. The normalized strain rate is thus equal to unity everywhere. We introduce infinitesimal perturbations $\tilde{T}_1$, μ_1, $\tilde{\dot{\gamma}}_1$ of temperature, reaction extent and strain rate, and study their evolution in time. The perturbation verifies the linearized system

$$\frac{\partial \tilde{T}_1}{\partial \tilde{t}} = \frac{\partial^2 \tilde{T}_1}{\partial \tilde{y}^2} + \mathbb{H}\left((\alpha + 1)\tilde{\dot{\gamma}}_1 - \beta\mu_1\right) - \mathbb{T}\frac{\partial \mu_1}{\partial \tilde{t}} \tag{53}$$

$$\frac{\partial \mu_1}{\partial \tilde{t}} = \mathbb{C}_T\tilde{T}_1 - \mathbb{C}_\mu \mu_1 \tag{54}$$

$$\alpha \frac{\partial \tilde{\dot{\gamma}}_1}{\partial \tilde{y}} - \beta \frac{\partial \mu_1}{\partial \tilde{y}} = 0 \qquad (55)$$

where we recall that

$$\alpha = \frac{\partial \tilde{\tau}}{\partial \tilde{\dot{\gamma}}}\Big|_{\tilde{\dot{\gamma}}_0, \mu_0} \qquad (56)$$

$$\beta = -\frac{\partial \tilde{\tau}}{\partial \mu}\Big|_{\tilde{\dot{\gamma}}_0, \mu_0} \qquad (57)$$

Equations (53), (54), and (55) form a linear system of partial differential equations. We look for solutions of the form

$$\begin{pmatrix} \tilde{T}_1 \\ \mu_1 \\ \tilde{\dot{\gamma}}_1 \end{pmatrix} = \begin{pmatrix} B_1 \\ B_2 \\ B_3 \end{pmatrix} \exp(s\tilde{t}) \exp(2\pi i \tilde{y}/\tilde{\lambda}) \qquad (58)$$

where s is the growth rate of the perturbation, $\tilde{\lambda} = \tilde{h}/N$ is the normalized wavelength, and where $\tilde{h}$ is the normalized layer thickness and N is an integer. The linear system has non-trivial solution $(B_1, B_2, B_3) \neq (0,0,0)$ if its determinant is identically zero; this condition gives a characteristic equation for the growth rate s:

$$\frac{\alpha}{\beta}\left(\frac{s + \mathbb{C}_\mu}{\mathbb{C}_T}\right)s + \frac{4\pi^2}{\tilde{\lambda}^2}\frac{\alpha}{\beta}\left(\frac{s + \mathbb{C}_\mu}{\mathbb{C}_T}\right) + s\mathbb{T}\frac{\alpha}{\beta} - \mathbb{H} = 0 \qquad (59)$$

The roots of the above quadratic equation are:

$$s(\lambda) = -\frac{1}{2}\left(\mathbb{C}_\mu + \frac{4\pi^2}{\tilde{\lambda}^2} + \mathbb{C}_T\mathbb{T}\right.$$
$$\left. \pm \sqrt{\left(\mathbb{C}_\mu + \frac{4\pi^2}{\tilde{\lambda}^2} + \mathbb{C}_T\mathbb{T}\right)^2 - \frac{16\pi^2\mathbb{C}_\mu}{\tilde{\lambda}^2} + 4\mathbb{H}\mathbb{C}_T\beta/\alpha}\right) \qquad (60)$$

When $\mathrm{Re}(s) < 0$, the perturbation decays exponentially in time and the spatially uniform solution is stable. Such a situation arises if

$$\tilde{\lambda} < \tilde{\lambda}_{\mathrm{cr}} = 2\pi\sqrt{\frac{\alpha\mathbb{C}_\mu}{\beta\mathbb{H}\mathbb{C}_T}} \qquad (61)$$

This defines a critical wavelength below which all perturbations vanish in time. In terms of dimensional parameters, the critical wavelength is

$$\lambda_{\mathrm{cr}} = 2\pi\frac{T_0}{T_a}\sqrt{\frac{d_{\mathrm{th}}}{\dot{\gamma}_0}\frac{\rho C T_a}{\tau_0}\frac{\alpha/\beta}{(1-\mu_0)}} \qquad (62)$$

If the initial deforming layer is thinner than λ_{cr}, a spatially homogeneous shear is stable and a constant shear zone thickness is a reasonable approximation. If the deforming layer is thicker than λ_{cr}, at the onset of the reaction, the deformation will localize to a thinner zone. The actual value of λ_{cr} is determined by the competition between heat diffusion and shear heating, as well as the ratio of rate hardening over reaction weakening effects. Large reaction weakening effect (parameter β) and shear heating (product $\tau_0\dot{\gamma}_0$) lead to a small critical wavelength. Concurrently, large rate strengthening and heat diffusivity tend to induce a large critical wavelength. The reaction kinetics enters via the activation temperature T_a: a higher T_a (i.e., a higher activation energy) induces a smaller λ_{cr}.

Using the numerical values reported in Table 1, the critical wavelength at the onset of the reaction ($\mu_0 = 0$) is $\lambda_{\mathrm{cr}} \approx 10$ m for a nominal strain rate of $\dot{\gamma}_0 = 10^{-9}$/s. At a strain rate of $\dot{\gamma}_0 = 10^{-6}$/s, the critical wavelength is $\lambda_{\mathrm{cr}} \approx 0.3$ m. Thus, if the initial shear zone is

1 m thick, localization of deformation is not expected to occur at the onset of the slip instability, but only at later stages during slip.

The importance of strain localization can also be addressed by rewriting the stability condition (Eq. (39)) in terms of a critical shear zone thickness h_{cr}. Instabilities arise if

$$h < h_{\mathrm{cr}} = \frac{\tau_0}{k}\frac{\tau_0\beta}{\rho C T_{\mathrm{eq}}^2/T_a + m_0\Delta H} \qquad (63)$$

For a high effective stiffness $k = 6 \times 10^8$ Pa/m (an initially stable configuration), the critical thickness is only $h_{\mathrm{cr}} \approx 0.65$ m. In Fig. 5, we observe that the slip rate (and thus the strain rate) at the onset of the reaction increases up to almost 10^{-7} m/s. At this strain rate, the stability analysis predicts a critical wave length threshold for unstable modes of the order of 0.1 m, which is lower than h_{cr}: the initially stable slip could thus become unstable due to localization of deformation in a narrower shear zone.

Although the linear stability analysis allows an analytical prediction of the smallest stable wavelength, we see in Eq. (60) that the growth rate s of the perturbation is an increasing function of the wavelength λ (Eq. (60)). In other terms, the instability mode with the highest growth rate corresponds to the largest wave length (i.e. equal to the layer thickness). In order to investigate the post-localization behavior and estimate the time evolution of the shear zone as the reaction progresses, it is necessary to perform a numerical, nonlinear stability analysis.

4.3 Long Term Behavior and Post-Localization Analysis. Here we adopt the frictional formulation of the constitutive law (Eq. (13)). In this case, the reference shear stress is $\tau_0 = f_0\sigma'$, the rate hardening coefficient is $\alpha = a/f_0$ and the reaction weakening parameter is $\beta = b/f_0$.

We model a $h = 1$ m thick layer of reacting rock sheared at a nominal strain rate $\dot{\gamma}_0 = 10^{-6}$ s^{-1} (a condition at which the weakening effect is still observed experimentally) at 30 km depth, for which we assume an initial temperature of 440 °C and an initial effective stress of around 400 MPa. The numerical values of the parameters used in the computations are reported in Table 1.

The governing equations for temperature (Eq. (50)), shear stress (Eq. (52)) and the full, nonlinear reaction kinetics (Eq. (4)) are solved by the method of lines. The space is discretised into uniform steps inside the layer (where deformation takes place) and logarithmically spaced steps outside the layer. We use MATLAB's solver ODE15S to integrate in time, and make use of the constrain that the average normalized strain rate throughout the layer is kept constant and equal to unity:
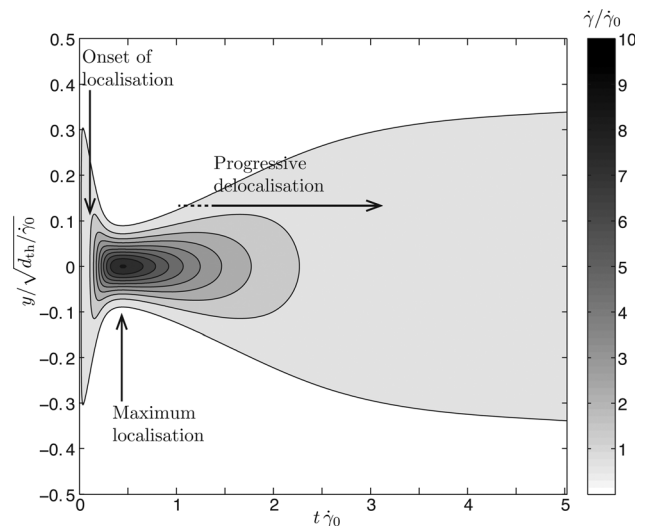

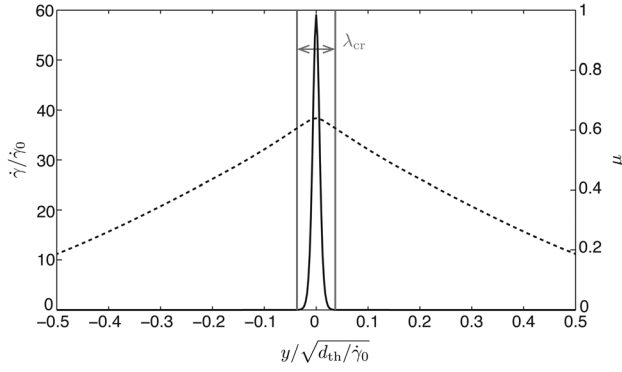**Fig. 6 Contours of strain rate as a function of time and space**

Fig. 7 Strain rate (solid line) and reaction extent (dotted line) profiles at the peak localization. The theoretical prediction is shown in red.

$$\frac{1}{h}\int_{-h/2}^{h/2}\tilde{\dot{\gamma}}\,dy = 1 \qquad (64)$$

Figure 6 displays the successive profiles of strain rate across the sheared layer as a function of time. As predicted by the linear stability analysis, localization occurs at early times. Localization does not persist in the layer because of the depletion of the reactant: we observe a subsequent "delocalization" of strain as the reactant is depleted. The profiles of strain rate and reaction extent are reported in Fig. 7 at the peak localization. Using the numerical values reported in Table 1, the theoretical prediction for the localization thickness computed using Eq. (62) is $\lambda_{cr} \approx 7.4$ cm. There is a reasonable agreement between the numerical result and the analytical prediction.

Starting from larger initial layer thickness does not change the peak localization thickness, except when the reaction is fully depleted before the thickness reaches its minimum.

5 Discussion

5.1 Effect of Pore Pressure. In the previous sections, we have considered a dry or drained layer of rock. However, it is interesting to discuss also the effect of pore fluid on slip stability. It is demonstrated in Ref. [23] that, in absence of dehydration reaction, thermal pressurisation of pore fluid alone is unlikely to induce slip instabilities in the rate strengthening regime. However, it was shown in Ref. [7] (e.g., Fig. 6), that dehydration reactions could induce slip instabilities for constant friction coefficient, and affect significantly the evolution of temperature and pore pressure during unstable slip. In this section we explore the possible importance of pore fluid pressurization in the strain localization process and slip instability compared to the reaction weakening effect.

5.1.1 Effect of Pore Pressure on Strain Localization. We explore first the effect of pore pressure on strain localization and wave length selection inside the sheared layer. Considering a fluid saturated rock layer, conservation of fluid mass leads to the following pore pressure generation/diffusion equation as derived in Ref. [7]:

$$\frac{\partial p}{\partial t} = \Lambda\frac{\partial T}{\partial t} + d_{hy}\frac{\partial^2 p}{\partial y^2} + m_w\frac{1-\xi}{\rho_f \beta^*}\frac{\partial \mu}{\partial t} \qquad (65)$$

where p is the pore pressure in the layer, Λ is the undrained thermoelastic pressurization coefficient [24], ρ_f is the pore fluid density, β^* is the elastic storage capacity of the rock, d_{hy} is the hydraulic diffusivity, m_w is the mass of water that is released due to the reaction per unit of rock volume (generally around 10% of m_0) and ξ is the ratio of pore volume creation to fluid volume

release due to the dehydration reaction. The friction law (Eq. 12) is written in terms of Terzaghi effective stress:

$$\tau = f(\sigma - p) = \left(f_0 + a\ln\frac{\dot{\gamma}}{\dot{\gamma}_0} - b\mu\right)(\sigma - p) \qquad (66)$$

The equilibrium equation $\partial\tau/\partial y = 0$ yields

$$\left(\frac{a}{\dot{\gamma}}\frac{\partial\dot{\gamma}}{\partial y} - b\frac{\partial\mu}{\partial y}\right)(\sigma - p) + \left(f_0 + a\ln\frac{\dot{\gamma}}{\dot{\gamma}_0} - b\mu\right)\frac{\partial p}{\partial y} = 0 \qquad (67)$$

At any given state of an undrained adiabatic spatially uniform deformation, the evolution in time of small perturbations regarding the strain rate, the pore fluid pressure, the temperature and the reaction extent is studied to determine the possibility of strain localization. Using the dimensionless variables defined by Eqs. (45)–(49) and $\tilde{p} = (p - p_0)/(\sigma - p_0)$ where p_0 is a reference pore pressure, the governing linearized system for the perturbation (Eqs. (53)–(55)) is modified to account for the pore pressure as follows:

$$\frac{\partial\tilde{p}_1}{\partial\tilde{t}} = \mathbb{D}\frac{\partial^2\tilde{p}_1}{\partial\tilde{y}^2} + \mathbb{B}\frac{\partial\tilde{T}_1}{\partial\tilde{t}} + \mathbb{P}\frac{\partial\mu_1}{\partial\tilde{t}} \qquad (68)$$

$$\frac{\partial\tilde{T}_1}{\partial\tilde{t}} = \frac{\partial^2\tilde{T}_1}{\partial\tilde{y}^2} + \mathbb{H}\big((\alpha+1)\tilde{\dot{\gamma}}_1 - \beta\mu_1 - \tilde{p}_1\big) - \mathbb{T}\frac{\partial\mu_1}{\partial\tilde{t}} \qquad (69)$$

$$\frac{\partial\mu_1}{\partial\tilde{t}} = \mathbb{C}_T\tilde{T}_1 - \mathbb{C}_\mu\mu_1 \qquad (70)$$

$$0 = \alpha\frac{\partial\tilde{\dot{\gamma}}_1}{\partial\tilde{y}} - \beta\frac{\partial\mu_1}{\partial\tilde{y}} - (1 - \beta\mu_0)\frac{\partial\tilde{p}}{\partial\tilde{y}} \qquad (71)$$

In the equations above, additional dimensionless numbers are introduced:

$$\mathbb{D} = d_{hy}/d_{th} \qquad (72)$$

$$\mathbb{B} = \Lambda T_a/(\sigma - p_0) \qquad (73)$$

$$\mathbb{P} = m_w\frac{1 - \xi}{\rho_f\beta*(\sigma - p_0)} \qquad (74)$$

The perturbations are here again decomposed into Fourier modes and solutions of the system presented in Eqs. (68)–(71) are searched in the form of

$$\begin{pmatrix}\tilde{p}_1 \\ \tilde{T}_1 \\ \mu_1 \\ \tilde{\dot{\gamma}}_1\end{pmatrix} = \begin{pmatrix}B_1 \\ B_2 \\ B_3 \\ B_4\end{pmatrix}\exp(s\tilde{t})\exp(2\pi i\tilde{y}/\tilde{\lambda}) \qquad (75)$$

where s is the growth rate of the perturbation and $\tilde{\lambda}$ is the normalized wavelength. By substituting the perturbation field Eq. (75) into the governing Eqs. (68)–(71) we obtain a homogeneous algebraic system for the coefficients B_i ($i = 1,4$). Thus a nonzero solution is possible only if the determinant of the linear system vanishes:

$$\det\begin{pmatrix} s + \mathbb{D}\frac{4\pi^2}{\tilde{\lambda}^2} & -\mathbb{B}s & -\mathbb{P}s & 0 \\ \mathbb{H} & s + \frac{4\pi^2}{\tilde{\lambda}^2} & \mathbb{H}\beta + \mathbb{T}s & -\mathbb{H}(1+\alpha) \\ 0 & -\mathbb{C}_T & s + \mathbb{C}_\mu & 0 \\ -(1 - \beta\mu_0) & 0 & -\beta & \alpha \end{pmatrix} = 0 \qquad (76)$$

This results in a characteristic polynomial equation of degree 3 for the growth coefficient s for which we look for roots with positive real part corresponding to a perturbation which grows

exponentially in time. We can again use Descartes' rule of signs to detect the signs of the roots. For $\beta > 0$, we find that the perturbations decay exponentially in time for

$$\tilde{\lambda} < \tilde{\lambda}_{\rm cr} = 2\pi\sqrt{\frac{\alpha\mathbb{C}_\mu}{\beta\mathbb{H}\mathbb{C}_T}} \tag{77}$$

which is exactly the same condition as in the drained case (Eq. (61)). This proves that pore pressure has no effect on strain localization in the reaction weakening regime. Note, however, that thermal pressurization itself has a localizing effect in absence of reaction weakening at very large strain rates [25–28]. In absence of chemical reaction ($\partial\nu/\partial t = 0$), the system degenerates and we retrieve a critical wavelength $\tilde{\lambda}_{\rm cr} = 2\pi\sqrt{\alpha(1+\mathbb{D})/(\mathbb{B}\mathbb{H})}$ compatible with the solution given by Refs. [26–28]. Figure 8 represents graphically the maximum real part of the growth rate $\tilde{s}$ as a function of the perturbation wavelength $\tilde{\lambda}$. The parameter values are taken from Table 1, and the hydraulic diffusivity was taken equal to the thermal diffusivity ($\mathbb{D} = 1$, a rather conservative estimate). The growth rate is always larger in the presence of thermal pressurization. For vanishingly small reaction weakening parameter β (but with the chemical effect on the pore pressure still included), a localization instability arises only when thermal pressurization is taken into account.

5.1.2 Effect of Pore Pressure on the Stability of the Spring-Slider System.
Using the notations in Eqs. (25)–(30), the governing linearized system for the perturbation (Eqs. (31)–(33) is modified to account for the pore pressure as follows:

$$\frac{\partial\tilde{p}_1}{\partial\tilde{t}} = -\mathbb{D}_{\rm hy}\tilde{p}_1 + \mathbb{B}\frac{\partial\tilde{T}_1}{\partial\tilde{t}} + \mathbb{P}\frac{\partial\mu_1}{\partial\tilde{t}} \tag{78}$$

$$\frac{\partial\tilde{T}_1}{\partial\tilde{t}} = \mathbb{H}((\alpha+1)\tilde{v}_1 - \beta\mu_1 - \tilde{p}_1) - \mathbb{T}\frac{\partial\mu_1}{\partial\tilde{t}} \tag{79}$$

$$\frac{\partial\mu_1}{\partial\tilde{t}} = \mathbb{C}_T\tilde{T}_1 - \mathbb{C}_\mu\mu_1 \tag{80}$$

$$-\mathbb{K}\tilde{v}_1 = \alpha\frac{\partial\tilde{v}_1}{\partial\tilde{t}} - \beta\frac{\partial\mu_1}{\partial\tilde{t}} - (1-\beta\mu_0)\frac{\partial\tilde{p}_1}{\partial\tilde{t}} \tag{81}$$

where $\mathbb{D}_{\rm hy} = d_{\rm hy}/(h_{\rm hy}v_\infty)$, with $h_{\rm hy}$ the characteristic hydraulic diffusion length (according to the membrane approximation, see
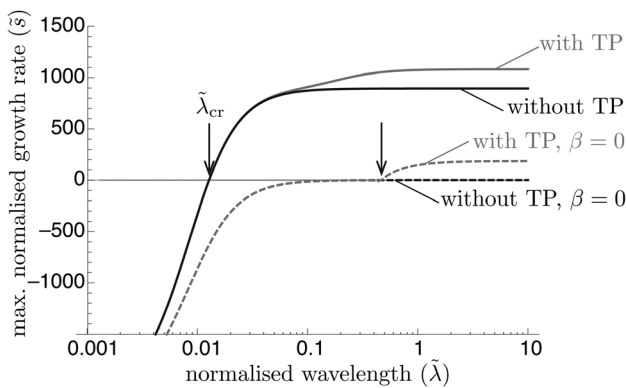

Fig. 8 Maximum real part of the normalized growth rate as a function of the normalized perturbation wavelength, computed from Eq. (76). Parameter values are reported in Table 1; hydraulic diffusivity is equal to thermal diffusivity. In the reaction weakening regime ($\beta > 0$, here $\beta = 0.83$, solid lines), thermal pressurization (TP) does not affect the stability condition and the critical wavelength. In absence of reaction weakening ($\beta = 0$, dotted lines), localization is driven by thermal pressurization (see Refs. [26–28]). The black dotted line never crosses the $\tilde{s} = 0$ line.

for instance Refs. [29, 30]). Looking for solutions of the linear differential system presented in Eqs. (78)–(81) of the form $B_i\exp(s\tilde{t})$, non-trivial solutions for the perturbations are found when the following determinant is identically zero:

$$\det\begin{pmatrix} s+\mathbb{D}_{\rm hy} & -\mathbb{B}s & -\mathbb{P}s & 0 \\ \mathbb{H} & s & \mathbb{H}\beta+\mathbb{T}s & -\mathbb{H}(1+\alpha) \\ 0 & -\mathbb{C}_T & s+\mathbb{C}_\mu & 0 \\ -(1-\beta\mu_0)s & 0 & -\beta s & \mathbb{K}+\alpha s \end{pmatrix} = 0 \tag{82}$$

In a similar way as in Sec. 3.2, Eq. (82) can be used to calculate a critical stiffness $\mathbb{K}_{\rm cr}$ below which the slip is unstable. In absence of chemical pressurization (for $\mathbb{P} = 0$), we note that thermal pressurization (parameter $\mathbb{B}$) has strictly no effect on the value of the critical stiffness. It confirms that thermal pressurization has a negligible effect on slip instabilities compared to rate-and-state effects [23]. Figure 9 reports the calculated non-dimensional critical stiffness $\mathbb{K}_{\rm cr}$ as a function of the chemical pressurization parameter $\mathbb{P}$ and for various hydraulic diffusivities (parameter $\mathbb{D}_{\rm hy}$). Using the parameter values given in Table 1 and $m_{\rm w} = 0.1\,m_0$, the parameter $\mathbb{P}$ is estimated to be 0.17 (in the shaded area of Fig. 9). In this range, the critical stiffness remains close to the one calculated without the effect of pore fluid; chemical pore fluid pressurization has thus a negligible effect. However, the critical stiffness significantly increases for values of $\mathbb{P}$ greater than 1 and low hydraulic diffusivities: this shows the contribution of chemical pore fluid pressurisation on slip stability in the rate-strengthening regime.

As expected, the drainage conditions have a major influence on the importance of pore fluid pressurization. However, permeability and thus fluid diffusivity remains largely unconstrained and is likely to be heterogeneous in space and time within fault rocks at depth. Although mainly phenomenological at this stage, the "intrinsic" reaction-weakening constitutive formulation described in this study is thus likely to be a more robust and general source of instability in reacting materials.

5.2 Applicability and Limits of the Model.

5.2.1 Choice of the Constitutive Law.
The constitutive formulation used in this study was stated in its most general assumptions in Eqs. (9)–(11). The main hypothesis is that the material weakens due to the chemical reaction. The weakening is assumed to be "intrinsic," in the sense that it is not related to a change in pore fluid pressure (such processes have been discussed in the previous section and in Ref. [7]). According to Refs. [8, 10], the intrinsic weakening can be due to the production of fine-grained olivine
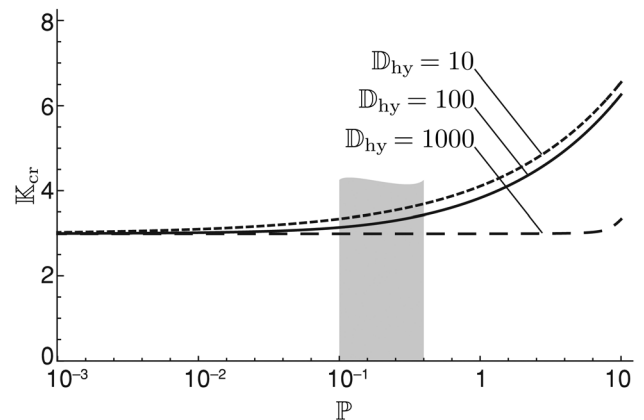

Fig. 9 Non-dimensional critical stiffness $\mathbb{K}_{\rm cr}$ as a function of chemical pressurisation parameter Π, for various hydraulic diffusivities. The shaded area corresponds to realistic values of Π. At low values of Π, the critical stiffness converges to a fixed value corresponding to the drained case.

products along microscopic shear zones, and to the creation of an important porosity that is easily compacted. These two processes have not been taken explicitly into account in the constitutive law assumed throughout the present study. In particular, the observed localization of fine grained olivine products along thin shear zones does *not* correspond to the strain localization determined by the calculations carried out in Sec. 4: the microscopic heterogeneities have been averaged out by assuming a global reaction weakening behavior. In that sense, the constitutive law is merely phenomenological, and a detailed micromechanical model would be needed to estimate the various contributions of the two mechanisms to the global observed weakening.

The stability analyses were performed using the linearized constitutive law, with no additional assumption on the actual form of the constitutive law. The analytical results are thus valid for any type of constitutive law that exhibits a velocity strengthening and reaction weakening behavior. We used a frictional law (Eq. (12)) in the numerical simulations of slip instability and strain localization. However, at elevated pressure and temperature, as it is the case at the conditions of serpentinite dehydration for instance, rocks are generally ductile and follow different constitutive models than friction laws [31,32]. Ductile rheological laws take into account the dependency of strength on physical conditions, including strain rate, confining pressure, temperature, grain size, pore pressure, or composition. There is currently no simple constitutive law that explicitly accounts for the reaction-weakening effect exhibited by Refs. [8, 10] (in particular, the weakening is observed to vanish at strain rate higher than 10^{-5}/s). An accurate description could potentially be done by integrating the effects of the mineral transformation in an effective medium model, using experimental constraints on the rheology of the pure end-members (in our case, serpentine and fine-grained olivine, if the data exist), following the approach of Ref. [33]. In addition, experiments could be done on partially dehydrated samples up to known reaction extents (for instance monitored by the mass of the sample), in order to relate directly the reaction extent to the measured strength.

Although the use of more detailed constitutive laws is required to study the nonlinear mechanical behavior of the shear zone during an instability, at this stage the phenomenological friction law constitutes a useful guide to establish the variety of behaviors expected at the onset of the reaction.

5.2.2 Role of the Reaction Kinetics. As emphasized by Eq. (39), the nucleation of slip instabilities depends on the reaction kinetics, and in particular of the activation temperature $T_a = E_a/R$. For very high activation energy and low equilibrium temperature T_{eq}, the term T_{eq}^2/T_a vanished in the expression of the critical stiffness (Eq. (39)), which implies that the reaction kinetics has no role in the actual stability condition. Physically, it corresponds to a situation in which the reaction kinetics is dramatically accelerated by slight temperature increases; the reaction is thus almost instantaneous, provided that there is enough heat provided in the system. Such a situation would arise when reactions are progressing under thermodynamic control.

In that case, the reaction rate is controlled by the ratio of mechanical energy dissipated in the shear zone over the reaction enthalpy. In the adiabatic approximation, the linear system governing the evolution of the perturbation $(\tilde{T}_1, \mu_1, \tilde{v}_1)$ is thus

$$\frac{\partial \tilde{T}_1}{\partial \tilde{t}} = 0 \tag{83}$$

$$\frac{\partial \mu_1}{\partial \tilde{t}} = \frac{\mathbb{H}}{\mathbb{T}}[(1+\alpha)\tilde{v}_1 - \beta\mu_1] \tag{84}$$

and

$$-\mathbb{K}\tilde{v}_1 = \alpha\frac{\partial \tilde{v}_1}{\partial \tilde{t}} - \beta\frac{\partial \mu_1}{\partial \tilde{t}} \tag{85}$$

The temperature is constant, since all the dissipated energy is converted into latent heat of reaction. Looking for solutions of the form $B_i \exp(s\tilde{t})$, we find that the growth factor is

$$s = \frac{-\mathbb{K}\mathbb{T} + \mathbb{H}\beta \pm \sqrt{(\mathbb{K}\mathbb{T} - \mathbb{H}\beta)^2 - 4\mathbb{H}\mathbb{K}\mathbb{T}\alpha\beta}}{2\alpha\mathbb{T}} \tag{86}$$

and hence the stability condition is

$$\mathbb{K} \geq \mathbb{K}_{cr} = \mathbb{H}\beta/\mathbb{T} \tag{87}$$

Remarkably, the inequality in Eq. (87) is strictly equivalent to the condition in Eq. (38) for negligible effect of depletion on the reaction kinetics. This confirms that the modeling approach described in this study can potentially be applied to reactions and phases changes occurring under thermodynamic control.

5.3 Relevance to Intermediate and Deep Earthquakes. The mechanical model presented in the present study is based on experimental observations of the apparent weakness of dehydrating serpentinite, independently from pore pressure effects [8–10]. Although mostly phenomenological, it captures the potential instabilities arising from the reaction-weakening behavior of rocks. Our model emphasizes the potential destabilizing effect of metamorphic reactions occurring at depth in the Earth. In particular, it has been argued that inter- mediate (70–300 km) and deep (300–700 km) focus earthquakes occurring along subductions zones could originate from mineral reactions and phase transitions, plastic instabilities or shear melting thermal runaway instabilities (e.g., Refs. [34–38]). The reaction-weakening behavior used in our model resembles the thermal runaway, except that the constitutive law is only indirectly temperature-dependent, through the thermal dependency of the reaction rate. In the case of serpentinite dehydration, we emphasize that the instabilities generated by the reaction do not rely on pore fluid pressurization. At low depth, generally below 40 km, dehydration of serpentine induces a positive total volume change, and thus chemical pore fluid pressurization also contributes to the generation of instabilities (see Sec. 5.1); however, at greater depth the total volume change is negative (see for instance Ref. [39]) and pore fluid pressure is expected to decrease (at least temporarily) during the reaction. The intrinsic reaction-weakening process assumed here is thus an interesting possibility for dehydration-induced earthquakes at intermediate depths.

Moreover, the slip instabilities arising during the mineral reaction can be short lived if the reactant is rapidly depleted (see Fig. 5): such transient slip events could correspond to slow slip events or low frequency earthquakes commonly observed in subduction zones (e.g., Refs. [40–43]).

We insist here that the reaction-weakening hypothesis is valid at the onset of the reaction only, since strain hardening and rate strengthening are also expected to increase during dehydration [10,12,13]. The evolution of fault motion during the instability itself would need to be constrained by numerical simulations including a more realistic rheology for the dehydrating material. In particular, it would be interesting to detect if the slip instabilities arising from the reaction-weakening process could be prolonged and/or maintained by thermo-chemical pore fluid pressurization.

6 Conclusion

The stability of fault slip in a reaction-weakening, rate-hardening material has been studied. The reaction-weakening feature is based on experimental deformation tests performed in drained conditions during serpentinite dehydration, and may originate from the formation of fine grained reaction products [8,10]. The stability condition is expressed in terms of critical stiffness of the surrounding medium, and mostly depends on the amplitude of the reaction-weakening effect, the reaction kinetics, the reaction

enthalpy and the ratio of ambient shear stress over shear zone thickness. The slip instabilities arising during the reaction have the following characteristics: (1) they are driven by shear heating through the temperature dependency of the kinetics, (2) they are independent from thermo-chemical pore fluid pressurization, and (3) they are expected to stop when the reactant is fully depleted. They constitute a reasonable candidate for intermediate and deep focus earthquakes, and support the hypothesis of transformation-induced faulting.

The stability analysis of homogeneous shear indicates that strain localization is expected during the reaction, down to a minimum finite wavelength. Numerical estimate of this wavelength yields values of the order of 0.1 to 1 m, depending on the strain rate and reaction kinetics. It is thus unlikely that localization bands can be seen in laboratory tests (indeed, Ref. [13] brings experimental evidences of homogeneous strain in serpentinite deformed during dehydration), but it is possible in the field at larger scale. The strain localization is also a destabilizing factor by itself, since it accelerates the macroscopic strain- weakening behavior of the rock during the reaction.

The model described in the present work is an attempt at understanding the possible consequences of metamorphism on the mechanical behavior of rocks. Although based on simple consititutive assumptions, it demonstrates that important effects are expected on the stability of deep fault zones. On the basis of experimental observations, more advanced constitutive models for reacting rocks will be developed in the future.

Acknowledgment

References

[1] Raleigh, C. B., and Paterson, M. S., 1965, "Experimental Deformation of Serpentinite and its Tectonic Implications," J. Geophys. Res.,70(16), pp. 3965–3985.

[2] Heard, H. C., and Rubey, W. W., 1966, "Tectonic Implications of Gypsum Dehydration," Geol. Soc. Am. Bull., 77, pp. 741–760.

[3] Murrell, S. A. F., and Ismail, I. A. H., 1976, "The Effect of Decomposition of Hydrous Minerals on the Mechanical Properties of Rocks," Tectonophysics, 31, pp. 207–258.

[4] Ko, S.-C., Olgaard, D. L., and Briegel, U., 1995, "The Transition from Weakening to Strengthening in Dehydrating Gypsum: Evolution of Excess Pore Pressures," Geophys. Res. Lett., 22(9), pp. 1009–1012.

[5] Milsch, H., and Scholz, C. H., 2005, "Dehydration-Induced Weakening and Fault Slip in Gypsum: Implications for the Faulting Process at Intermediate Depth in Subduction Zones," J. Geophys. Res., 110, B04202.

[6] Wong, T.-F., Ko, S.-C., and Olgaard, D. L., 1997, "Generation and Maintenance of Pore Pressure Excess in a Dehydrating System 2. Theoretical Analysis," J. Geophys. Res., 102(B1), pp. 841–852.

[7] Brantut, N., Sulem, J., and Schubnel, A., 2011, "Effect of Dehydration Reactions on Earthquake Nucleation: Stable Sliding, Slow Transient and Unstable Slip," J. Geophys. Res., 116, B05304.

[8] Rutter, E. H., and Brodie, K. H., 1988, "Experimental 'Syntectonic' Dehydration of Serpentinite Under Conditions of Controlled Pore Water Pressure," J. Geophys. Res., 93(B5), pp. 4907–4932.

[9] Rutter, E. H., and Brodie, K. H., 1995, "Mechanistic Interactions Between Deformation and Metamorphism," Geol. J., 30, pp. 227–240.

[10] Arkwright, J. C., Rutter, E. H., Brodie, K. H., and Llana-Fúnez, S., 2008, "Role of Porosity and Dehydration Reactions on the Deformation of Hot-Pressed Serpentinite Aggregates," J. Geol. Soc. (London), 165, pp. 639–649.

[11] Rutter, E. H., Llana-Fùnez, S., and Brodie, K. H., 2009, "Dehydration and Deformation of Intact Cylinders of Serpentinite," J. Struct. Geol., 31, pp. 29–43.

[12] Hirose, T., Bystricky, M., Kunze, K., and Stünitz, H., 2006, "Semi-Brittle Flow during Dehydration of Lizardite-Chrysotile Serpentinite Deformed in Torsion: Implication for the Rheology of Oceanic Lithosphere," Earth Planet. Sci. Lett., 249, pp. 484–493.

[13] Chernak, L. J., and Hirth, G., 2010, "Deformation of Antigorite Serpentinite at High Temperature and Pressure," Earth Planet. Sci. Lett., 29, pp. 23–33.

[14] Sulem, J., and Famin, V., 2009, "Thermal Decomposition of Carbonates in Fault Zones: Slip-Weakening and Temperature-Limiting Effects," J. Geophys. Res., 114, B03309.

[15] Brantut, N., Schubnel, A., Corvisier, J., and Sarout, J., 2010, "Thermochemical Pressurization of Faults During Coseismic Slip," J. Geophys. Res., 115, B05314

[16] Baumberger, T., Berthoud, P., and Caroli, C., 1999, "Physical Analysis of the State- and Rate-Dependent Friction Law. II. Dynamic Friction," Phys. Rev. B, 60(6), pp. 3928–3939.

[17] Rice, J. R., Lapusta, N., and Ranjith, K., 2001, "Rate and State Dependent Friction and the Stability of Sliding between Elastically Deformable Solids," J. Mech. Phys. Solids, 49, pp. 1865–1898.

[18] Nakatani, M., 2001, "Conceptual and Physical Clarification of Rate and State Friction: Frictional Sliding as a Thermally Activated Rheology," J. Geophys. Res., 106(B7), pp. 13347–13380.

[19] Holland, T. J. B., and Powell, R., 1998, "An Internally Consistent Thermodynamic Data Set for Phases of Petrological Interest," J. Metamorph. Geol., 16, pp. 309–343.

[20] Evans, B. W., 2004, "The Serpentinite Multisystem Revisited: Chrysotile is Metastable," Int. Geol. Rev., 24(6), pp. 479–506.

[21] Llana-Fúnez, S., Brodie, K. H., Rutter, E. H., and Arkwright, J. C., 2007, "Experimental Dehydration Kinetics of Serpentinite using Pore Volumometry," J. Metamorph. Geol., 25, pp. 423–438.

[22] Moore, D. E., Lockner, D. A., Shengli, M., Summers, R., and Byerlee, J. D., 1997, "Strengths of Serpentinite Gouges at Elevated Temperatures," J. Geophys. Res., 102(B7), pp. 14787–14801.

[23] Segall, P., and Rice, J. R., 2006, "Does Shear Heating of Pore Fluid Contribute to Earthquake Nucleation?," J. Geophys. Res., 111, B09316

[24] Rice, J. R., 2006, "Heating and Weakening of Faults during Earthquake Slip," J. Geophys. Res., 111, B05311.

[25] Rice, J. R., and Rudnicki, J. W., 2004, "Stability of Spatially Uniform, Adiabatic, Undrained Shear of a Fault Zone," unpublished manuscript.

[26] Platt, J. D., Rice, J. R., and Rudnicki, J. W., 2010, "Strain Localization within a Fluid-Saturated Fault Gouge Layer during Seismic Shear, Abstract T31D-03," Proceedings of the 2010 Fall Meeting, AGU, Dec. 13–17, San Francisco, CA.

[27] Rice, J. R., Rudnicki, J. W., and Tsai, V. C., 2005, "Shear Localization in Fluid-Saturated Fault Gouge by Instability of Spatially Uniform, Adiabatic, Undrained Shear," Eos Trans. AGU 86(52), Fall Meeting Supplement, Abstract No. T13E-05.

[28] Platt, J. D., Brantut, N., and Rice, J. R., 2011, "Strain Localization Driven by Thermal Decomposition During Seismic Shear," oral presentation at the 2011 fall meeting, AGU, Dec. 5–9, San Francisco, CA.

[29] Segall, P., and Rice, J. R., 1995, "Dilatancy, Compaction, and Slip Instability of a Fluid-Infiltrated Fault," J. Geophys. Res., 100(B11), pp. 22155–22171.

[30] Garagash, D. I., and Rudnicki, J. W., 2003, "Shear Heating of a Fluid-Saturated Slip-Weakening Dilatant Fault Zone 1. Limiting Regimes," J. Geophys. Res., 108(B2), 2121.

[31] Walker, A. N., Rutter, E. H., and Brodie, K. H., 1990, "Experimental Study of Grain-Size Sensitive Flow of Synthetic, Hot-Pressed Calcite Rocks," Geol. Soc. Spec. Publ. (London) 54, pp. 259–284.

[32] Tullis, T. E., Horowitz, F. G., and Tullis, J., 1991, "Flow Laws of Polyphase Aggregates from End-Member Flow Laws," J. Geophys. Res., 96(B5), pp. 8081–8096.

[33] Liu, M., 1997, "A Constitutive Model for Olivine-Spinel Aggregates and its Application to Deep Earthquake Nucleation," J. Geophys. Res., 102(B3), pp. 5295–5312.

[34] Kirby, S. H., 1987, "Localized Polymorphic Phase Transformations in High-Pressure Faults and Applications to the Physical Mechanism of Deep Earthquakes," J. Geophys. Res., 92(B13), pp. 13789–13800.

[35] Hobbs, B. E., and Ord, A., 1988, "Plastic Instabilities: Implications for the Origin of Intermediate and Deep Focus Earthquakes," J. Geophys. Res., 93(B9), pp. 10521–10540.

[36] Frohlich, C., 1989, "The Nature of Deep-Focus Earthquakes," Annu. Rev. Earth Planet. Sci., 17, pp. 227–254.

[37] Green, H. W., and Houston, H., 1995, "The Mechanics of Deep Earthquakes," Annu. Rev. Earth Planet. Sci., 23, pp. 169–213.

[38] John, T., Medvedev, S., Rüpke, L. H., Andersen, T. B., Podladchikov, Y. Y., and Austreim, H., 2009, "Generation of Intermediate-Depth Eathquakes by Self-Localizing Thermal Runaway," Nat. Geosci., 2, pp. 137–140.

[39] Green, H. W., and Marone, C., 2002, "Instability of Deformation, Plastic Deformation of Rocks," Rev. Mineral. Geochem., 51(1), pp. 181–199.

[40] Hirose, H., Hirahara, K., Kimata, F., Fujii, N., and Miyazaki, S., 1999, "A Slow Thrust Slip Event Following the two 1996 Hyuganada Earthquakes beneath the Bungo Channel, Southwest Japan," Geophys. Res. Lett., 26(21), pp. 3237–3240.

[41] Dragert, H., Wang, K., and James, T. S., 2001, "A Slient Slip Event on the Deeper Cascadia Subduction Zone," Science, 292, pp. 1525–1528.

[42] Rogers, G., and Dragert, H., 2003, "Episodic Tremor and Slip on the Cascadia Subduction Zone: The Chatter of Silent Slip," Science, 300, pp. 1942–1943.

[43] Obara, K., Hirose, H., Yamamizu, F., and Kasahara, K., 2004, "Episodic Slow Slip Events Accompanied by Non-Volcanic Tremors in Southwest Japan Subduction Zone," Geophys. Res. Lett., 31, L23602.